Contemporary Mathematics
http://ojs.wiserpub.com/index.php/CM/

Research Article

Three-Dimensional Multiphase Peristaltic Flow Through a Porous Medium with Compliant Boundary Walls

Nouman Ijaz[1], Ahmed Zeeshan[2], Safia Batool[1], M. M. Bhatti[3*], Kh. S. Mekheimer[4]

[1] Department of Mathematics and Statistics, University of Lahore, (Sargodha Campus) Sargodha 40100, Pakistan
[2] Department of Mathematics and Statistics, FBAS, International Islamic University, Islamabad 44000, Pakistan
[3] Material Science, Innovation and Modelling (MaSIM) Research Focus Area, North-West University, Mafikeng Campus, Mmabatho, South Africa
[4] Department of Mathematics, Faculty of Science (Men), Al-Azhar University, Nasr-City, Cairo, Egypt
E-mail: mmbhatti@sdust.edu.cn

Received: 20 May 2024; **Revised:** 26 September 2024; **Accepted:** 14 October 2024

Abstract: In this communication, we focus on the peristaltic propulsion of multiphase fluid flowing in a three-dimensional rectangular channel with compliant walls. The flow is influenced by porosity and magnetic effects, and the formulation is based on lubrication theory. The governing equations for both fluid and particulate phases are derived for continuity and momentum, assuming a long wavelength $(\lambda \to \infty)$ and a creeping flow regime $(R_e \to 0)$. Exact solutions of the partial differential equations for both solid and liquid velocities are obtained using the eigenfunction expansion method. We analyze the influence of several relevant parameters on the velocities and profiles graphically. It is found that fluid velocity increases with greater damping and mass effects. Conversely, wall tension and wall elastance have an inverse effect on velocity distribution. While wall tension tends to reduce the size of the boluses, wall stiffness tends to enhance the trapping of boluses. Additionally, the size of the trapped bolus increases due to the combined effects of the magnetic field and porosity.

***Keywords*:** multi-phase flow, magnetohydrodynamics, peristaltic flow, porous medium, compliant wall

MSC: 76A05, 76S05, 76W05

Abbreviation

$\overline{U}, \overline{V}, \overline{W}$	Velocity components
$\overline{X}, \overline{Y}, \overline{Z}$	Coordinate axis
x, y, z	Dimensionless coordinate axis
t	Time
$\overline{p}$	Fluid pressure
S	Stress tensor
D	Drag force
k	Porosity

DOI: https://doi.org/10.37256/cm.5420244994

c	Wave velocity
a	Channel's half-width
b	Amplitude
B_0	Magnetic field strength
h	Non-Dimensional wave
R_e	Reynolds number
M_1	Suspension parameter
M	Magnetic field

Greek symbols

χ_1	Jeffrey parameter
μ	Viscosity of the fluid
ρ	Fluid density
ρ	Particle volume fraction
λ	Wavelength
η_1	Wall rigidity
η_2	Wall tension
η_3	Mass characterizing
η_4	Damping nature
η_5	Wall elastance
ϕ	Amplitude ratio
$\dot{\Upsilon}$	Rate of strain
$\ddot{\Upsilon}$	Retardation time
τ_t	Elastic tension
τ_m	Mass of the wall per unit area
τ_d	Viscous damping
τ_b	Fexural rigidity
τ_k	Spring stiffness

Subscripts

p	Particle phase
f	Fluid phase

1. Introduction

The motion of fluid within a flexible channel (either circular or cylindrical) follows the principle of peristaltic pumping. Peristalsis refers to the rhythmic contraction and relaxation of smooth walls in a sinusoidal wave pattern. This mechanism is essential in various biological processes, such as the transport of urine from the kidneys to the bladder, the movement of food through the esophagus, spermatozoa transport, the motility of the chyme in the intestines, and natural oscillations within blood vessels. These examples illustrate the pervasive role of peristalsis in the human body.

From a mathematical and theoretical perspective, the analysis of peristaltic flow poses significant challenges, particularly when accounting for viscous fluid behavior. Historically, the complexity of the governing equations has hindered precise analytical solutions. However, with the introduction of various physical approximations, such as long-wavelength and low-Reynolds number assumptions, researchers have been able to make substantial progress in understanding peristaltic transport. These approximations simplify the mathematical modeling, allowing for more tractable solutions and providing deeper insights into the underlying fluid dynamics.

In recent years, the study of both Newtonian and non-Newtonian fluids in peristaltic transport through tubes has expanded significantly. Non-Newtonian fluids-such as blood, paint, and biological fluids-exhibit complex flow characteristics, deviating from the classical Newtonian behavior. The study of these fluids is of paramount importance in industrial processes and biological systems, where understanding their flow dynamics can lead to advancements in medical technologies and engineering applications.

Mekheimer and Abd Elmaboud [1] investigated the mechanics of peristaltic motion in a fluid suspension containing small particles within a channel, utilizing a regular perturbation series to solve the problem. Akram et al. [2] analyzed the effects of lateral wall motion on the sinusoidal movement of small particles in a three-dimensional setup, incorporating slip conditions. Nadeem et al. [3] explored the three-dimensional peristaltic flow mechanism using the lubrication approach and provided a perturbation solution. Ellahi et al. [4] examined the influence of mass transfer on peristaltic motion in a non-uniformly heated rectangular channel. Zeeshan et al. [5] studied peristaltic propulsion in a duct with bio-rheological fluids, deriving exact solutions for the flow by solving the governing partial differential equations using the method of separation of variables.

Prakash et al. [6] focused on the peristaltic pumping of nanofluids through a tapered channel in a porous medium, with applications in blood flow. Shit et al. [7] analyzed the pulsatile flow and heat transfer of blood in an overlapping vibrating atherosclerotic artery using numerical methods. Nazeer et al. [8] presented an analytical study on heat transfer in peristaltic flow through an asymmetric channel, considering laser and magnetic effects as a potential remedy for autoimmune diseases. Choudhari et al. [9] investigated the multiple slip effects on magnetohydrodynamic (MHD) peristaltic blood flow of a Phan-Thien-Tanner nanofluid through an asymmetric channel.

Peristaltic propulsion of non-Newtonian fluids is of particular importance in magnetohydrodynamics (MHD), which has applications in controlling diseases such as cancer through its influence on human organs. MHD peristaltic flow is also critical in various physical and industrial processes, though it remains highly nonlinear and complex to model. Riaz et al. [10] discussed the peristaltic motion of a Carreau fluid under MHD in a rectangular channel with flexible walls, obtaining results through graphical and physical parameter analysis. Hayat et al. [11] provided numerical results for peristaltic motion in a rotating channel by solving the governing equations. Ellahi et al. [12] studied the peristaltic flow of a Williamson fluid in a rectangular channel, finding that peristaltic pumping amplifies the propagation of sinusoidal waves, leading to fluid flow instability. Numerical methods were employed to describe the pressure effects in such fluids, and significant work has been done on the small intestine to observe peristaltic flow.

Xu et al. [13] examined electro-osmotic flow through a divergent channel, with applications in drug delivery systems. Shah et al. [14] studied magnetized pulsatile blood flow through a porous tube under non-localized shear stress conditions. Narla et al. [15] conducted a thermal analysis of peristaltic flow with electro-osmotic effects in microchannels. Bhandari et al. [16] utilized a kinematic membrane transient model in conjunction with a viscoplastic model to examine periodic contractions in microchannels. Further related studies can be found in references [17–19].

Motivated by the advancements in the literature and the significance of such flows, this study investigates the influence of solid particles and magnetic fields on the peristaltic motion of an incompressible, laminar, non-Newtonian Jeffrey fluid in a duct embedded with a porous medium. This research has broad applications in fluid machinery, including solid machine pumps, toxic chemical transport, dust-fluid tube pumps, and medical devices such as heart-lung and dialysis machines, which are based on peristaltic flow principles. The formulation of the problem is based on lubrication theory, with the governing equations for both the fluid and particulate phases derived under the assumptions of a long wavelength ($\lambda \to \infty$) and a creeping flow regime ($R_e \to 0$). Exact solutions for the solid-liquid velocities are obtained using the Eigen-function expansion method. The effects of several key parameters on velocity profiles are analyzed graphically, providing insights into the behavior of both fluid and particle phases. Detailed graphical results highlight the critical dynamics and their potential applications.

2. Governing modelling

Consider a Jeffrey fluid with small particles suspended in a three-dimensional porous channel. The Jeffrey fluid is characterized by its irrotational flow, constant density, and incompressibility. A symmetric peristaltic wave, described by a sinusoidal function, propagates through the three-dimensional channel, as illustrated in Figure 1. The sinusoidal wave moves with a speed c, has a wavelength λ, and an amplitude b, all under the influence of an applied magnetic field.

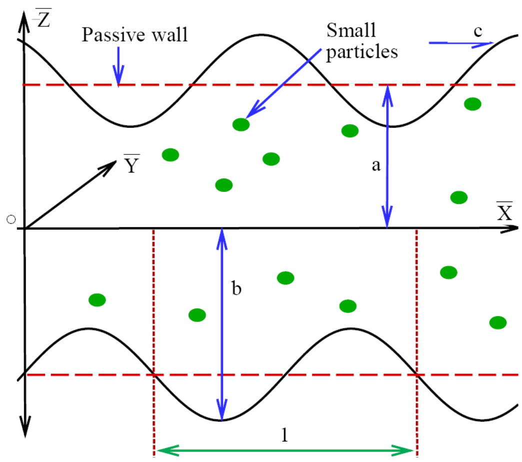

Figure 1. Structure of the particle-fluid peristaltic motion

The geometric configuration is aligned along the $\overline{Z}$-axis and $\overline{X}$-axis in the vertical and horizontal directions, respectively, while the $\overline{Y}$-axis is oriented laterally. The mathematical representation of the peristaltic wave can be expressed as:

$$\overline{H}(\overline{X},\, t) = Z = \pm a \pm b \sin\alpha, \;\; \alpha = k_l\left(\overline{X} - ct\right), \;\; k_l = \frac{2\pi}{\lambda}, \tag{1}$$

where a the channel's half-width, and t the time.

The leading equations for the fluid- and particulate phases in the current formulation are written as [20, 21]:

$$\frac{\partial \overline{U}_f}{\partial \overline{X}} + \frac{\partial \overline{W}_f}{\partial \overline{Z}} = 0, \tag{2}$$

$$\rho_f\left(\frac{\partial \overline{U}_f}{\partial t} + \overline{W}_f\frac{\partial \overline{U}_f}{\partial \overline{Z}} + \overline{U}_f\frac{\partial \overline{U}_f}{\partial \overline{X}}\right) = -\frac{\partial \overline{p}}{\partial \overline{X}} + \frac{\partial}{\partial \overline{X}}\xi_{XX} + \frac{\partial}{\partial \overline{Y}}\xi_{XY} + \frac{\partial}{\partial \overline{Z}}\xi_{XZ}$$

$$- \frac{\sigma B_0^2 \overline{U}_f}{(1-\rho)} + \frac{\rho D\left(\overline{U}_p - \overline{U}_f\right)}{(1-\rho)} - \frac{\mu \overline{U}_f}{k_1(1-\rho)}, \tag{3}$$

where ρ the density, D the drag force, $\overline{p}$ the pressure, ρ the particle volume fraction, σ the electrical conductivity, k the porous parameter, μ the viscosity of particle-fluid mixture, and p, f in the subscripts are particulate- and fluid-phase.

$$\rho_f\left(\frac{\partial \overline{W}_f}{\partial t}+\overline{U}_f\frac{\partial \overline{W}_f}{\partial \overline{X}}+\overline{W}_f\frac{\partial \overline{W}_f}{\partial \overline{Z}}\right)=-\frac{\partial \overline{p}}{\partial \overline{Z}}+\left(\frac{\partial}{\partial \overline{X}}\xi_{\overline{ZX}}+\frac{\partial}{\partial \overline{Y}}\xi_{\overline{ZY}}+\frac{\partial}{\partial \overline{Z}}\xi_{\overline{ZZ}}\right)$$

$$+\frac{\rho D\left(\overline{U}_p-\overline{U}_f\right)}{(1-\rho)}. \tag{4}$$

The proposed equations for particulate-phase read as:

$$\frac{\partial \overline{U}_p}{\partial \overline{X}}+\frac{\partial \overline{W}_p}{\partial \overline{Z}}=0, \tag{5}$$

$$\rho_f\rho\left(\frac{\partial \overline{U}_p}{\partial t}+\overline{U}_p\frac{\partial \overline{U}_p}{\partial \overline{X}}+\overline{W}_p\frac{\partial \overline{U}_p}{\partial \overline{Z}}\right)=-\rho\frac{\partial \overline{p}}{\partial \overline{X}}+\rho D\left(\overline{U}_f-\overline{U}_p\right), \tag{6}$$

$$\rho_f\rho\left(\frac{\partial \overline{W}_p}{\partial t}+\overline{U}_p\frac{\partial \overline{W}_p}{\partial \overline{X}}+\overline{W}_p\frac{\partial \overline{W}_p}{\partial \overline{Z}}\right)=-\rho\frac{\partial \overline{p}}{\partial \overline{Z}}+\rho D\left(\overline{W}_f-\overline{W}_p\right). \tag{7}$$

The drag coefficient D, and the viscosity suspension μ using empirical relation is contemplated as

$$D=\frac{9\mu_0}{2\tilde{a}_r^2}\chi(\rho),\ \ \chi(\rho)=\frac{4+3\left[\sqrt{8\rho-3\rho^2}+\rho\right]}{(3\rho-2)^2},$$

$$\mu=\frac{\mu_0}{1-\kappa\rho},\ \ \kappa=0.07e^{\dfrac{2.49\rho+1107e^{-1.69\rho}}{T}}, \tag{8}$$

where the radius of every suspended particle is $\tilde{a}_r$, μ_0 the fluid viscosity, and T the absolute temperature. The precised value of particle volume fraction $\rho=0.6$ was determined by Charm and Kurland [22] via cone and plate viscometer.

In Eqs. (2) and (3), the Jeffrey fluid is used as the base fluid tensor, as described by [23]:

$$\xi=\frac{\mu}{1+\chi_1}\left(\dot{\Upsilon}+\chi_2\ddot{\Upsilon}\right), \tag{9}$$

where χ_1 represents the ratio of the relaxation time to the retardation time, χ_2 is the delay time, and $\dot{\Upsilon}$ denotes the shear rate. The dot notation indicates the first derivative with respect to time, while $\ddot{\Upsilon}$ represents the second derivative. The transformation for the above equations from fixed to wave frame are

$$u^\dagger=\overline{U}-c,\ \overline{W}=w^\dagger,\ x^\dagger=\overline{X}-tc,\ y^\dagger=\overline{Y},\ \overline{Z}=z^\dagger,\ \overline{p}=p^\dagger, \tag{10}$$

Inaugurating the dimensionless variables for further formulation:

$$x=\frac{x^{\dagger}}{\lambda},\ w=\frac{w^{\dagger}}{\delta c},\ t=\frac{tc}{\lambda},\ h=\frac{\overline{H}}{a}, y=\frac{y^{\dagger}}{d},\ z=\frac{z^{\dagger}}{a},\ p=\frac{\delta a p^{\dagger}}{\mu c},\ \delta=\frac{a}{\lambda},\ u=\frac{u^{\dagger}}{c},$$

$$\beta=\frac{a}{d},\ R_e=\frac{ac\rho}{\mu},\ \xi_{xx}=\frac{a}{\mu c}\xi_{\overline{XX}},\ \xi_{yz}=\frac{d}{\mu c}\xi_{\overline{YZ}},\ \xi_{zz}=\frac{\lambda}{\mu c}\xi_{\overline{ZZ}},\ \xi_{yy}=\frac{\lambda}{\mu c}\xi_{\overline{YY}},$$

$$\xi_{xz}=\frac{a}{\mu c}\xi_{\overline{XZ}},\ \xi_{xy}=\frac{d}{\mu c}\xi_{\overline{XY}}, \tag{11}$$

where R_e stands for Reynolds number. Make a use of Eq. (11) in Eq. (1) to Eq. (9), and contemplating the lubrication approach, the formulated equations for fluid-phase found as

$$\frac{dp}{dx}=\frac{\beta^2}{1+\chi_1}\frac{\partial^2 u_f}{\partial y^2}+\frac{1}{1+\chi_1}\frac{\partial^2 u_f}{\partial z^2}-\frac{u_f+1}{k}-M^2(u_f+1)+\rho M_1(u_p-u_f), \tag{12}$$

The above equation reduced for Newtonian fluid by contemplating the value of $\chi_1=0$. In Eq. (12) M_1 the suspension parameter, k the porosity parameter, M the Hartmanm number. These parameters are found as:

$$M_1=\frac{a^2 D}{(1-\rho)\mu},\ k=\frac{k_1}{(1-\rho)d^2},\ M=\sqrt{\frac{\sigma}{(1-\rho)\mu}}aB_0. \tag{13}$$

The particulate-phase equations reduced as

$$\frac{1}{1-\rho}\frac{dp}{dx}=M_1(u_f-u_p). \tag{14}$$

The boundary conditions in dimensionless format as

$$u_f(x,\ y,\ z)=-1,\ \ y=\pm 1,$$

$$u_f(x,\ y,\ z)=-1,\ \ z=\pm h(x)=\pm(1+\phi\sin 2\pi x). \tag{15}$$

where the amplitude ratio is $\phi\ (=b/a)$.

The following is the condition for the compliant peristaltic flow:

$$\overline{L}=-\tilde{p}_0+\overline{p}, \tag{16}$$

where $\tilde{p}_0$ denotes the pressure towards the rectangular duct because of the muscle's tension. The $\overline{L}$ operator for the compliant boundary wall is defined as [24]:

$$\overline{L} = \tau_m \frac{\partial^2}{\partial t^2} + \tau_d \frac{\partial}{\partial t} - \tau_t \frac{\partial^2}{\partial \overline{X}^2} + \tau_b \frac{\partial^4}{\partial \overline{X}^4} + \tau_k, \tag{17}$$

where τ_t the elastic tension, τ_m the mass of the wall per unit area, τ_d the viscous damping, τ_b the flexural rigidity of the plate, and τ_k the spring stiffness.

Using Eq. (17), the pressure gradient after employing the dimensionless variables can be written as:

$$\frac{dp}{dx} = \eta_1 \frac{\partial^3 \Lambda}{\partial x^3} + \eta_2 \frac{\partial^3 \Lambda}{\partial x \partial t^2} + \eta_3 \frac{\partial^2 \Lambda}{\partial x \partial t} + \eta_4 \frac{\partial^5 \Lambda}{\partial x^5} + \eta_5 \frac{\partial \Lambda}{\partial x}, \tag{18}$$

where Λ is presented in Eq. (15).

The non-dimensional parameters ξ_i, $(i = 1, \cdots 5)$ are defined as

$$\eta_1 = -\frac{\tau_t a^3}{\lambda^3 \mu c}, \quad \eta_2 = \frac{\tau_m c a^3}{\mu \lambda^3}, \quad \eta_3 = \frac{\tau_d a^3}{\mu \lambda^2}, \quad \eta_3 = \frac{\tau_b a^3}{\mu \lambda c}, \quad \eta_5 = \frac{\tau_k a^3}{\lambda c \mu}, \tag{19}$$

where η_1 the wall rigidity, η_2 the wall tension, η_3 the mass characterizing, η_4 the damping nature of the compliant wall, and η_5 the wall elastance.

3. Analytical solutions using eigen-function expansion method

The formulated equations are linear and can therefore be solved exactly. We have a second-order, linear, homogeneous partial differential equation, subject to homogeneous boundary conditions. Consequently, the method of separation of variables is applied. We assume that

$$v(y,\ z) = Y(y) \times Z(z), \tag{20}$$

$$\frac{Y''}{Y} = \frac{-1}{\beta^2}\frac{Z''}{Z} + \frac{M^2}{\beta^2}(1 + \lambda_1) = -\alpha^2(\text{say}) \tag{21}$$

$$\Rightarrow \frac{Y''}{Y} = -\alpha^2 \tag{22}$$

$$-\alpha^2 = \frac{-1}{\beta^2}\frac{Z''}{Z} + \frac{M^2}{\beta^2}(1 + \lambda_1). \tag{23}$$

$$0 = [Y(\pm 1)] \times [Z(z)],\ \Rightarrow Y\ (\pm 1) = 0. \tag{24}$$

Therefore, there are two possible cases to obtain the required solution:

$$\frac{Y''}{Y} = -\alpha^2, \;\Rightarrow\; \left[D^2 + \alpha^2\right] \times Y(y) = 0, \;\Rightarrow\; D = \pm(i\alpha). \tag{25}$$

$$Y(y) = c_1 \cos(\alpha y) + c_2 \sin(\alpha y). \tag{26}$$

Now, applying the boundary conditions mentioned above yields:

$$c_2 = 0. \tag{27}$$

Therefore, the eigenvalues are:

$$\alpha_n = \left(\frac{(2n-1)\pi}{2}\right), \quad \text{for } n = 1, 2, 3... \tag{28}$$

The necessary eigenfunctions are:

$$Y(y) = c_1 \cos\left(\frac{\pi(2n-1)y}{2}\right). \tag{29}$$

The exact solutions of Eq. (12) and Eq. (14) are given by:

$$\begin{aligned} u_f =& \frac{1}{(\rho-1)A_1}\left[k - (\rho-1)(A_1+k)\cosh\frac{\sqrt{A_1}A_2 z}{\sqrt{k}}\frac{\sqrt{A_1}A_2 h}{\sqrt{k}}\right] \\ & \times\left[4\cos A_3 z \cosh\frac{y}{\beta}\sqrt{A_3^2 + \left(\frac{1}{k}+M^2\right)A_2^2}\right. \\ & \left.\times\left\{1 + k - (A_1(\rho-1)+k)\cosh\frac{\sqrt{A_1}A_2 z}{\sqrt{k}}\frac{\sqrt{A_1}A_2 h}{\sqrt{k}}\right\} \div (\rho-1)A_1\right] \\ & \div\frac{\frac{y}{\beta}\sqrt{A_3^2 + \left(\frac{1}{k}+M^2\right)A_2^2}\sin A_3 h}{2A_3\left(h + \frac{\sin 2hA_3}{2A_3}\right)}, \end{aligned} \tag{30}$$

$$A_1 = 1 + k(1+M^2), \;\; A_2 = \sqrt{1+\varsigma_1}, \;\; A_3 = \frac{2n-1}{2}\pi z, \tag{31}$$

$$u_p = \frac{1}{(\rho-1)A_1}\left[k-(\rho-1)(A_1+k)\cosh\frac{\sqrt{A_1}A_2 z}{\sqrt{k}}\frac{\sqrt{A_1}A_2 h}{\sqrt{k}}\right]$$

$$\times\left[4\cos A_3 z\cosh\frac{y}{\beta}\sqrt{A_3^2+\left(\frac{1}{k}+M^2\right)A_2^2}\right.$$

$$\left.\times\left\{1+k-(A_1(\rho-1)+k)\cosh\frac{\sqrt{A_1}A_2 z}{\sqrt{k}}\frac{\sqrt{A_1}A_2 h}{\sqrt{k}}\right\}\div(\rho-1)A_1\right]$$

$$\div\frac{\frac{y}{\beta}\sqrt{A_3^2+\left(\frac{1}{k}+M^2\right)A_2^2}\sin A_3 h}{2A_3\left(h+\frac{\sin 2hA_3}{2A_3}\right)}-\frac{}{M_1(1-\chi_1)}. \tag{32}$$

4. Graphical results and discussion

This section presents the graphical results for various parameters affecting the governing flow dynamics. The influence of parameters such as solid particle concentration in the fluid, ρ, Hartmann number, M, suspension parameter, M_1, porous parameter, k, wall rigidity, η_1, wall tension, η_2, mass characterization, η_3, damping coefficient of the compliant wall, η_4, and wall elastance, η_5, are analyzed. For computational analysis, we have chosen the following parameter values: $M = 1$, $M_1 = 1$, $k = 1$, $\eta_1 = 0.8$, $\eta_2 = 0.5$, $\eta_3 = 0.01$, $\eta_4 = 0.5$, $\varphi = 0.1$, and $\eta_5 = 0.5$.

To validate our findings, we compared them with previously published data from Nadeem et al. [25], using $\rho = 0$ as the comparison parameter. The results demonstrate excellent agreement, as depicted in Figure 2. This figure not only highlights the strong correlation between the two sets of results but also reinforces the accuracy and reliability of our present work.

In Figure 3, the behavior of small particles is examined. It is observed that an increase in the particle volume fraction, ρ, leads to a reduction in fluid velocity, as well as a similar deceleration in particle velocity. Furthermore, Figure 3b shows that particle velocity decreases near the walls, demonstrating the influence of particle concentration in boundary layers.

Figure 4 illustrates the effect of porosity on the velocity profile. An increase in the porous parameter k significantly enhances the velocity in the central region of the channel, while the velocity near the walls shows a contrasting reduction. This behavior can be attributed to the influence of porous medium resistance near the walls, promoting flow in the channel's core.

As shown in Figure 5, the presence of a magnetic field exerts a significant opposing effect on both fluid and particle velocities. The magnetic field induces a Lorentz force, which acts to resist fluid motion, a phenomenon previously reported by Zeeshan et al. [26]. Similarly, Figure 6 reveals that increasing the wall rigidity parameter, η_1, introduces additional resistance, thereby slowing down both fluid and particle motion. This result is consistent with observations from Ellahi et al. [27], who studied couple stress fluid flow in three dimensions.

In Figure 7, it is demonstrated that increasing wall tension, η_2, causes a reduction in the velocities of both the fluid and particles. Figure 8 explores the effect of the mass characterization parameter, η_3, on velocity profiles. It is found that increasing η_3 enhances both fluid and particle velocities, with particle velocity exhibiting slightly higher magnitudes compared to fluid velocity.

The damping effect of the compliant wall, η_4, and wall elastance, η_5, are analyzed in Figure 9-10. Both parameters significantly enhance fluid and particle velocities, likely due to their role in reducing resistance from the wall's motion.

The next important phenomenon investigated is fluid trapping, represented by the size of boluses in the flow, visualized using streamlines. Trapping is of engineering and physiological significance as it can lead to recirculation zones, which in biological systems may contribute to thrombosis or in reactive fluids, undesired chemical transformations. Figure 11-15 illustrate this trapping mechanism.

From Figure 11, it is clear that a stronger magnetic field reduces the size of the trapped boluses, while increasing their number. Figure 12 shows that while the porous parameter k affects the bolus size, it does not influence the number of boluses. In Figure 13, the increase in wall rigidity, η_1, suppresses the size of the boluses, a behavior similarly observed for increasing wall tension, η_2, as shown in Figure 14. Finally, in Figure 15, it is noted that increasing both mass characterization, η_3, and the damping nature of the compliant wall, η_4, leads to a reduction in the size of the trapped bolus.

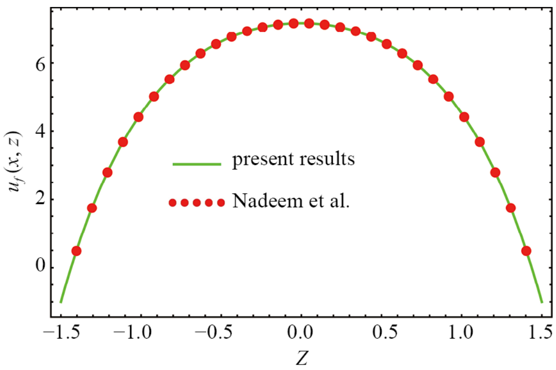

Figure 2. Comparison of the present results with $\rho = 0$, $M = 0$, $k \to \infty$ against the published results of Nadeem et al. [25]

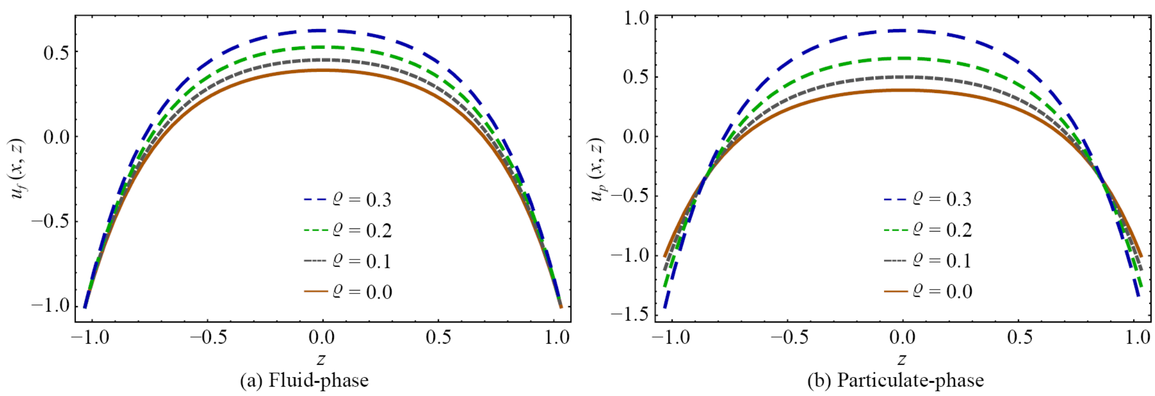

Figure 3. Consequences of ρ on velocity distribution

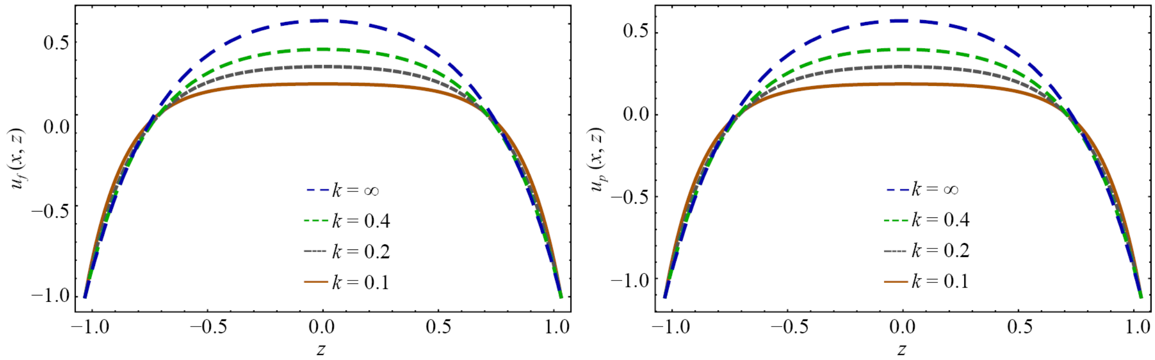

(a) Fluid-phase (b) Particulate-phase

Figure 4. Consequences of k on velocity distirbution

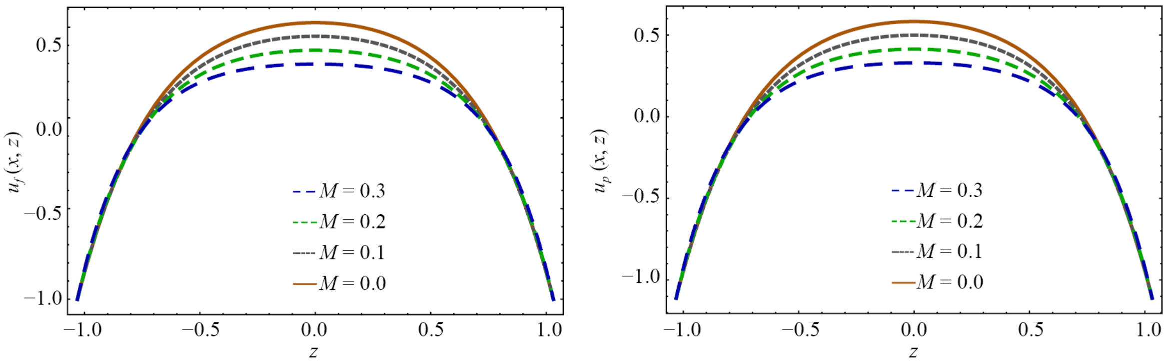

(a) Fluid-phase (b) Particulate-phase

Figure 5. Consequences of M on velocity distirbution

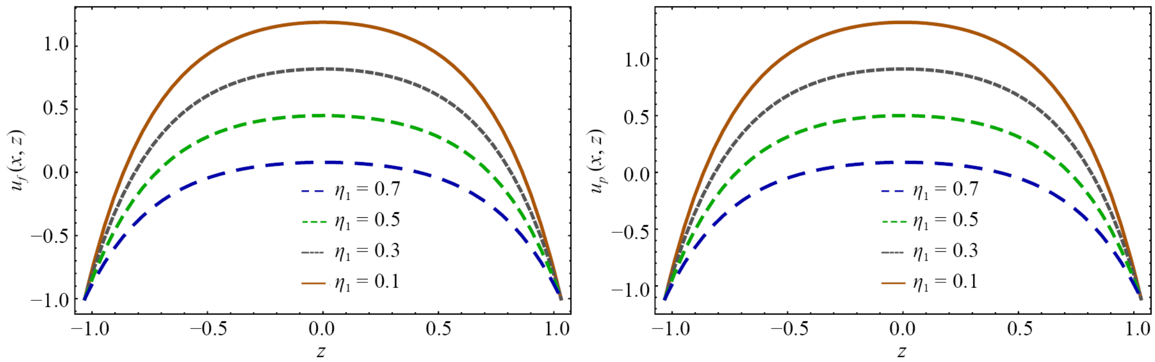

(a) Fluid-phase (b) Particulate-phase

Figure 6. Consequences of η_1 on velocity distirbution

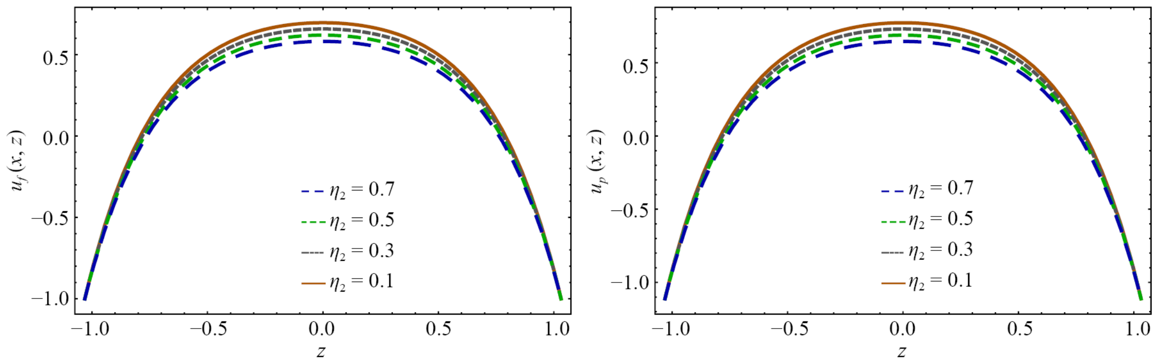

(a) Fluid-phase (b) Particulate-phase

Figure 7. Consequences of η_2 on velocity distirbution

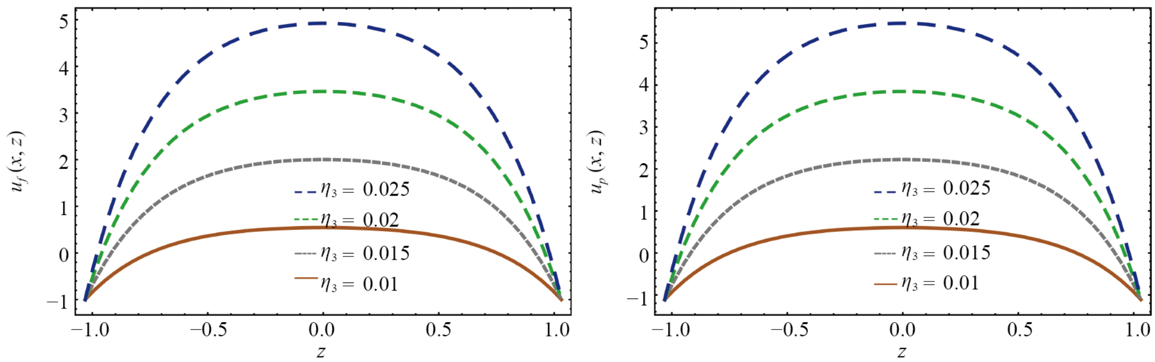

(a) Fluid-phase (b) Particulate-phase

Figure 8. Consequences of η_3 on velocity distirbution

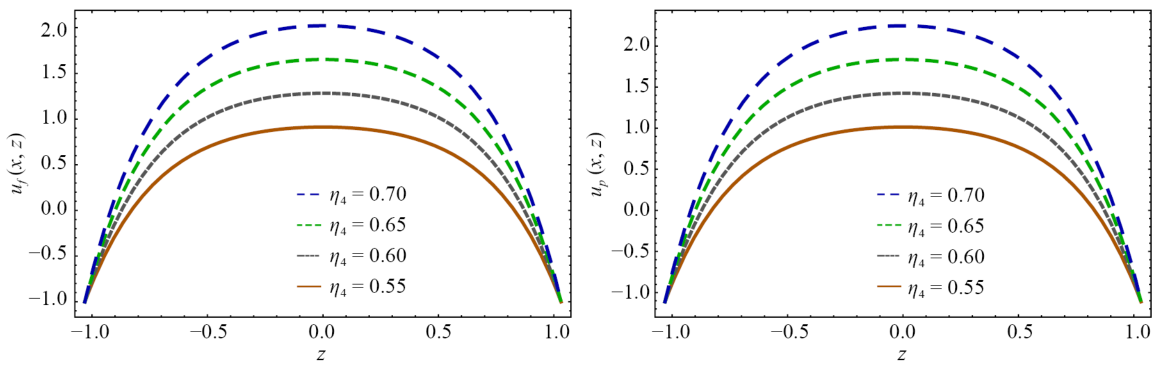

(a) Fluid-phase (b) Particulate-phase

Figure 9. Consequences of η_4 on velocity distirbution

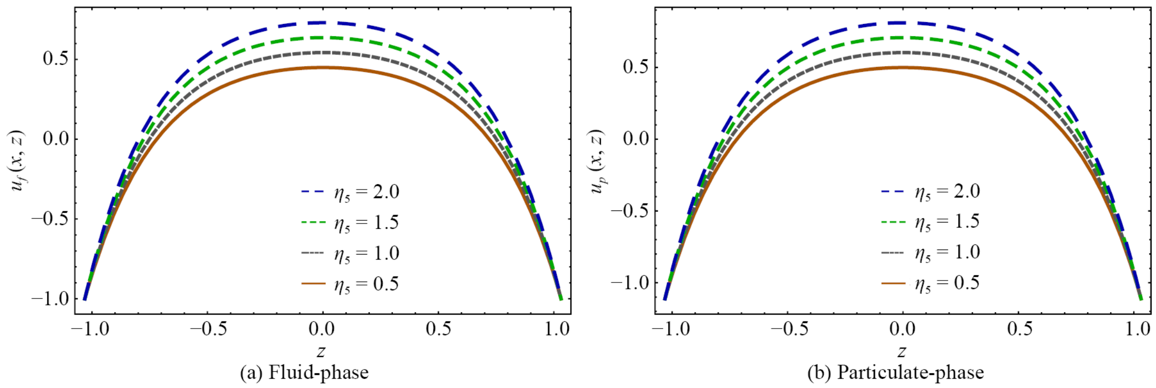

Figure 10. Consequences of η_5 on velocity distirbution

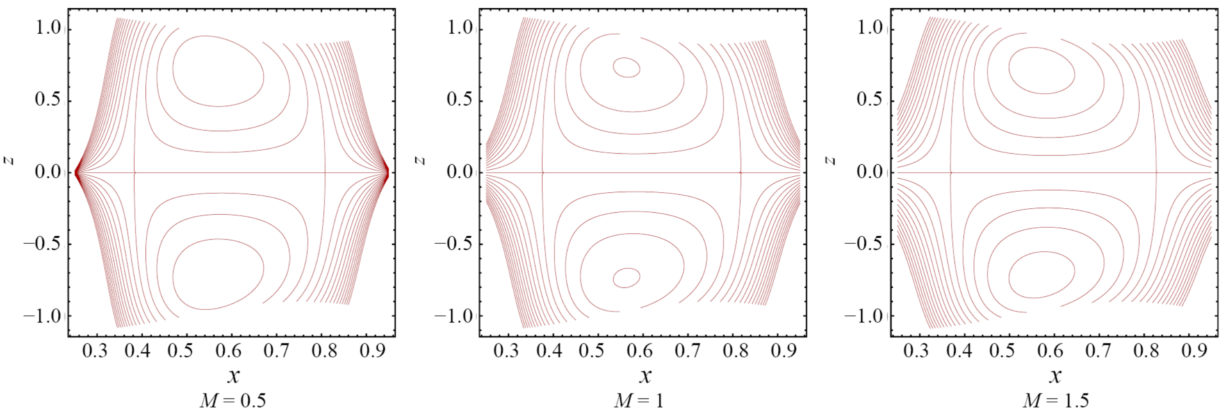

Figure 11. Streamlines phenomena against distinct values k

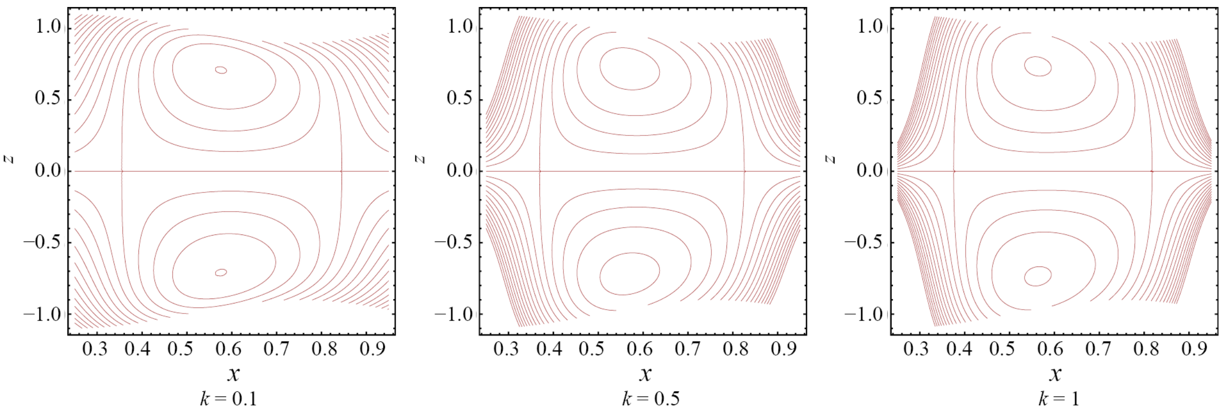

Figure 12. Streamlines phenomena against distinct values η_1

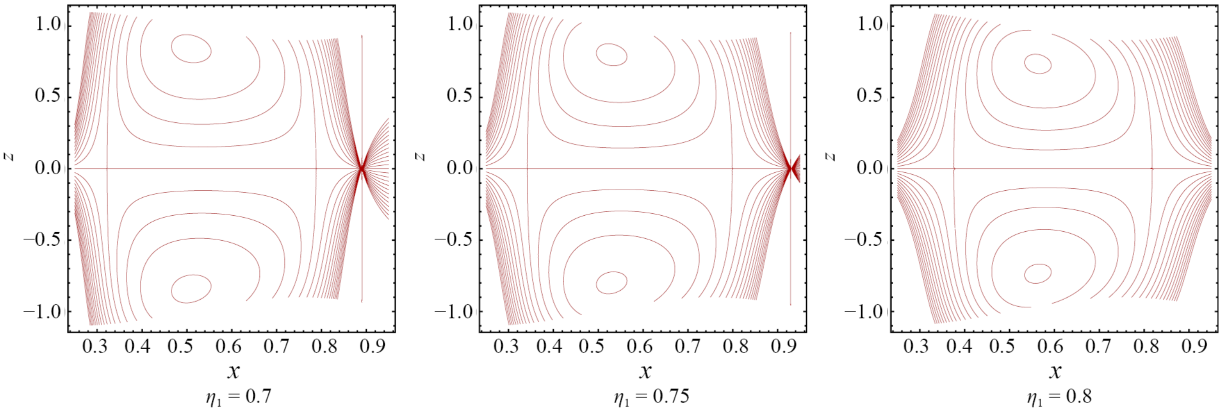

Figure 13. Streamlines phenomena against distinct values η_2

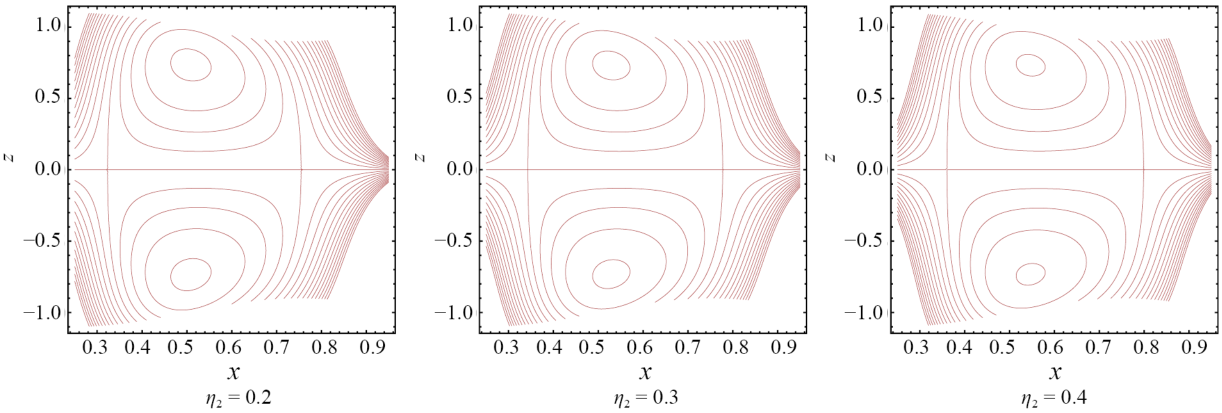

Figure 14. Streamlines phenomena against distinct values η_3

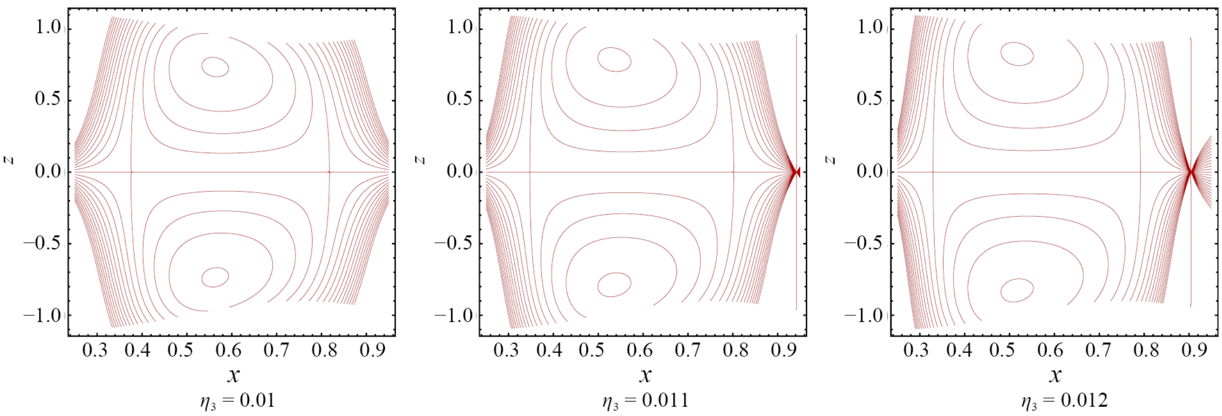

Figure 15. Streamlines phenomena against distinct values k

5. Conclusions

In this article, we analyzed the effects of a magnetic field on peristaltically induced flow of a Jeffrey fluid within a rectangular channel with porous and compliant walls. The governing equations for both the fluid and particle phases were derived using lubrication theory. The Eigenfunction expansion method was employed to solve the resulting partial differential equations, and the solutions were obtained in an exact form. The key findings of this study are summarized as follows:

(i) The presence of a magnetic field and increased wall rigidity reduces the velocity distribution, while higher particle volume fraction and increased porosity enhance the velocity.

(ii) It was observed that increasing the damping effect and mass characterization parameter leads to an increase in fluid velocity.

(iii) The relationship between wall tension and wall elastance demonstrates opposing effects on velocity distribution, where wall tension decreases velocity, while elastance tends to enhance it.

(iv) The size of the trapped bolus increases under stronger magnetic fields and higher porosity, contributing to a more pronounced trapping effect.

(v) Wall rigidity intensifies the trapping bolus, while higher wall tension reduces both the size and occurrence of boluses.

(vi) Damping characteristics of the compliant wall and wall elastance significantly influence the size of the trapped boluses.

(vii) The present results for a viscous fluid can be recovered by setting $\chi_1 = 0$.

Conflict of interest

The authors declare no competing financial interest.

References

[1] Mekheimer KS, Elmaboud YA. Peristaltic transport of a particle-fluid suspension through a uniform and non-uniform annulus. *Applied Bionics and Biomechanics*. 2008; 5(2): 47-57.

[2] Akram S, Mekheimer KS, Abd Elmaboud Y. Particulate suspension slip flow induced by peristaltic waves in a rectangular duct: Effect of lateral walls. *Alexandria Engineering Journal*. 2018; 57(1): 407-414.

[3] Nadeem S, Akram S, Hayat T, Hendi AA. Peristaltic flow of a Carreau fluid in a rectangular duct. *Journal of Fluids Engineering*. 2012; 134(4): 041201.

[4] Ellahi R, Bhatti MM, Vafai K. Effects of heat and mass transfer on peristaltic flow in a non-uniform rectangular duct. *International Journal of Heat and Mass Transfer*. 2014; 71: 706-719. Available from: https://doi.org/10.1016/j.ijheatmasstransfer.2013.12.038.

[5] Zeeshan A, Ijaz N, Bhatti M, Mann A. Mathematical study of peristaltic propulsion of solid-liquid multiphase flow with a biorheological fluid as the base fluid in a duct. *Chinese Journal of Physics*. 2017; 55(4): 1596-1604.

[6] Prakash J, Tripathi D, Tiwari AK, Sait SM, Ellahi R. Peristaltic pumping of nanofluids through a tapered channel in a porous environment: applications in blood flow. *Symmetry*. 2019; 11(7): 868.

[7] Shit GC, Maiti S, Roy M, Misra J. Pulsatile flow and heat transfer of blood in an overlapping vibrating atherosclerotic artery: A numerical study. *Mathematics and Computers in Simulation*. 2019; 166(2019): 432-450.

[8] Nazeer M, Irfan M, Hussain F, Siddique I, Khan MI, Guedri K, et al. Analytical study of heat transfer rate of peristaltic flow in asymmetric channel with laser and magnetic effects: Remedy for autoimmune disease. *International Journal of Modern Physics B*. 2022: 37(03): 2350025.

[9] Choudhari R, Baleanu D, Vaidya H, Prasad K, Khan MI, Bafakeeh OT, et al. Analysis of multiple slip effects on MHD blood peristaltic flow of Phan-Thien-Tanner nanofluid through an asymmetric channel. *International Journal of Modern Physics B*. 2023; 37(11): 2350102.

[10] Riaz A, Ellahi R, Nadeem S. Peristaltic transport of a Carreau fluid in a compliant rectangular duct. *Alexandria Engineering Journal*. 2014; 53(2): 475-484.
[11] Hayat T, Zahir H, Tanveer A, Alsaedi A. Numerical study for MHD peristaltic flow in a rotating frame. *Computers in Biology and Medicine*. 2016; 79(C): 215-221.
[12] Ellahi R, Riaz A, Nadeem S. Three dimensional peristaltic flow of Williamson fluid in a rectangular duct. *Indian Journal of Physics*. 2013; 87(12): 1275-1281.
[13] Xu YJ, Nazeer M, Hussain F, Khan MI, Hameed M, Shah NA, et al. Electro-osmotic flow of biological fluid in divergent channel: Drug therapy in compressed capillaries. *Scientific Reports*. 2021; 11(1): 1-13.
[14] Shah NA, Al-Zubaidi A, Saleem S. Study of magnetohydrodynamic pulsatile blood flow through an inclined porous cylindrical tube with generalized time-nonlocal shear stress. *Advances in Mathematical Physics*. 2021; 2021: 1-11. Available from: https://doi.org/10.1155/2021/5546701.
[15] Narla V, Tripathi D, Bhandari D. Thermal analysis of micropolar fluid flow driven by electroosmosis and peristalsis in microchannels. *International Journal of Ambient Energy*. 2022; 43(1): 8193-8205.
[16] Bhandari DS, Tripathi D, Narla VK. Transient membrane kinematic model for viscoplastic fluids: Periodic contraction in the microchannel. *The European Physical Journal Special Topics*. 2022; 232(3): 1-10.
[17] Raza M, Ellahi R, Sait SM, Sarafraz M, Shadloo MS, Waheed I. Enhancement of heat transfer in peristaltic flow in a permeable channel under induced magnetic field using different CNTs. *Journal of Thermal Analysis and Calorimetry*. 2019; 140(7): 1-15.
[18] Turkyilmazoglu M, Siddiqui AA. The instability onset of generalized isoflux mean flow using Brinkman-DarcyBénard model in a fluid saturated porous channel. *International Journal of Thermal Sciences*. 2023; 188: 108249. Available from: https://doi.org/10.1016/j.ijthermalsci.2023.108249.
[19] Turkyilmazoglu M. Advective flow in a magnetized layer of fluid between hydro-thermal slippery parallel walls. *Archive of Applied Mechanics*. 2023; 93(12): 4351-4360.
[20] Shah NA, Vieru D, Fetecau C. Effects of the fractional order and magnetic field on the blood flow in cylindrical domains. *Journal of Magnetism and Magnetic Materials*. 2016; 409: 10-19. Available from: https://doi.org/10.1016/j.jmmm.2016.02.013.
[21] Riaz A, Ahammad NA, Alqarni M, Hejazi HA, Tag-ElDin EM. Peristaltic flow of a viscous fluid in a curved duct with a rectangular cross section. *Frontiers in Physics*. 2022; 10: 1-12. Available from: https://doi.org/10.3389/fphy.2022.961201.
[22] Charm SE, Kurland GS. *Blood Flow and Microcirculation*. USA: Wiley; 1974.
[23] Ishtiaq F, Ellahi R, Bhatti MM, Alamri SZ. Insight in thermally radiative cilia-driven flow of electrically conducting non-Newtonian Jeffrey fluid under the influence of induced magnetic field. *Mathematics*. 2022; 10(12): 1-21.
[24] Srinivas S, Kothandapani M. The influence of heat and mass transfer on MHD peristaltic flow through a porous space with compliant walls. *Applied Mathematics and Computation*. 2009; 213(1): 197-208.
[25] Nadeem S, Riaz A, Ellahi R. Peristaltic flow of a Jeffrey fluid in a rectangular duct having compliant walls. *Chemical Industry and Chemical Engineering Quarterly*. 2013; 19(3): 399-409.
[26] Zeeshan A, Bhatti M, Muhammad T, Zhang L. Magnetized peristaltic particle-fluid propulsion with Hall and ion slip effects through a permeable channel. *Physica A: Statistical Mechanics and Its Applications*. 2020; 550: 123999. Available from: https://doi.org/10.1016/j.physa.2019.123999.
[27] Ellahi R, Bhatti MM, Fetecau C, Vafai K. Peristaltic flow of couple stress fluid in a non-uniform rectangular duct having compliant walls. *Communications in Theoretical Physics*. 2016; 65(1): 66.